Amanna and Rakshit
Biotechnology for the Environment (2025) 2:2
https://doi.org/10.1186/s44314-025-00018-5

Biotechnology for the Environment

RESEARCH

Open Access

Pretreatment of polyethylene terephthalate (PET) using physicochemical methods and their effects on biodegradation

Ruth Amanna[1,2] and Sudip K. Rakshit[1,2,3*]

Abstract

Recently, biodegradation has gained importance as a potential solution to alleviate pollution. This study dives into the physicochemical transformations of polyethylene terephthalate (PET) to enhance biodegradation efficiency. PET films were subjected to pretreatments, including UV irradiation, thermal oxidation, size reduction, and a combination of thermal oxidation and size-reduction pretreatments. These pretreated samples were then biodegraded using either an immobilized enzyme or the whole-cell *Thermobifida fusca* YX. The physicochemical effects of these treatments were evaluated through techniques such as attenuated total reflectance Fourier transform infrared (ATR-FTIR) spectroscopy, scanning electron microscopy (SEM), and weight-loss analysis. The findings revealed that UV irradiation caused repetitive cycles of photo-oxidation over 3 h, which impaired biodegradation due to increased crystallinity. Conversely, thermal oxidation improved biodegradation up to an optimal temperature of 80 °C. Higher temperatures were favorable for whole-cell biodegradation, while slightly lower temperatures (70–80 °C) were optimal for enzyme-mediated processes. A similar trend was observed for thermally oxidized size-reduced particles, with the smallest particle size exhibiting the highest biodegradation rates, 21.25 ± 0.24% with the immobilized enzyme and 16.61 ± 0.63% with whole cells. The study further demonstrated that all pretreatments primarily targeted the ester linkage, specifically the C = O and C–H bonds. Additionally, the effects of pretreatments were tested on chemical hydrolysis. Due to its inherently caustic nature, chemical hydrolysis did not require any pretreatment. These findings shed light on the interplay of physical and chemical factors influencing biodegradation, offering valuable insights into the importance of pretreatments for the biological hydrolysis of such polymers.

Keywords PET pretreatments, UV irradiation, Thermal oxidation, Size reduction, PET Biodegradation

*Correspondence:
Sudip K. Rakshit
srakshit@lakeheadu.ca
Full list of author information is available at the end of the article

Graphical Abstract

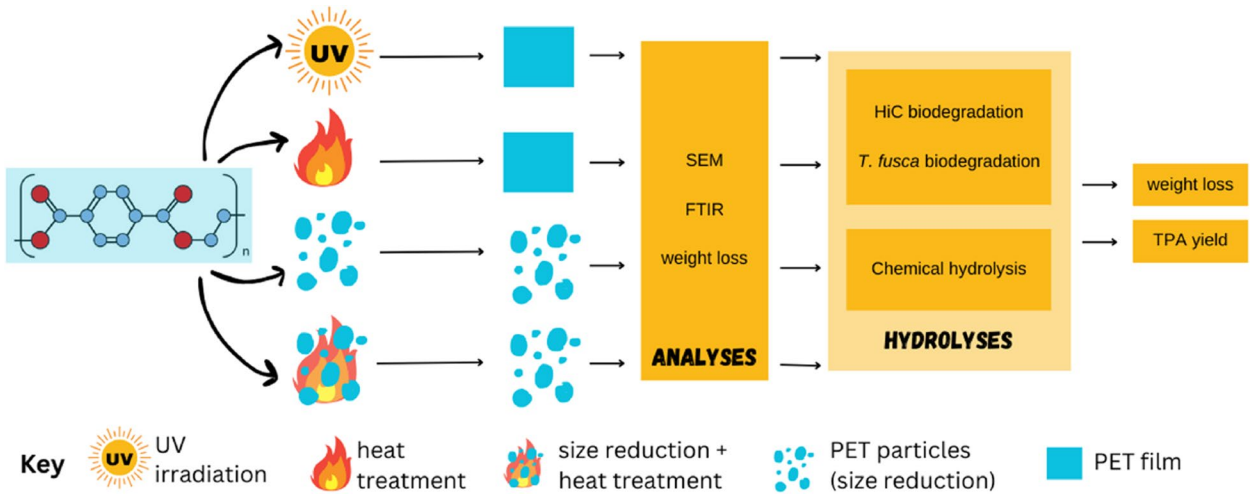

Introduction

Since its invention in 1941, the production and consumption of polyethylene terephthalate (PET) based products has skyrocketed. The desirable properties of PET include its inertness, transparent nature, flexibility, and the availability of cheap monomers, albeit from fossil resources. Hence, it has been used for the mass production of a list of products including water bottles, containers, textile fibers, and packaging material [1]. However, these very attributes have made PET inert to break down and ubiquitous in modern life. Its accumulation has resulted in substantial environmental issues [2, 3]. In 2021, 390.7 million metric tons of plastics were produced globally, of which 6.2% was PET [4]. In 2022, Canada recycled an average of 110,359 tonnes of the 243,743 tonnes of rigid PET waste, meaning that only 45% of the rigid PET was recycled [5]. Each year, more than 300 million metric tons of plastic waste are globally produced [6]. As a result of these challenges, many countries are looking for ways to solve the serious plastic pollution issue by developing methods to reuse plastics, thereby coming closer to a circular economy [4, 7]. Many countries are increasingly using their unrecycled plastic waste for energy recovery [8]. Unfortunately, these processes generate numerous toxic and hazardous compounds [9–13]. Managing over nine billion metric tons of plastics [14] currently on our planet into a sustainable circular economy is a challenge that needs to be addressed urgently.

A circular economy requires the reuse of presently discarded end-of-use plastics to produce new plastic items. The currently used recycling technology involves melting PET products after use, followed by its use for other lower-value products. This is because melts lead to plastics of different functionality like reduced mechanical and optical properties and allows migration of nonintentional added substances into food and pharmaceutical products, thus limiting the application of PET in this way [15–18]. An efficient circular economic method would break down the waste PET into its monomeric constituents, terephthalic acid (TPA) and ethylene glycol (EG). This would eliminate the issue of migration of chemicals into PET, generating high-quality recycled PET from waste PET.

Chemical hydrolysis is one such method that can depolymerize PET to TPA and EG. A recent study developed and optimized a chemical hydrolysis process that was able to hydrolyze used single-use PET bottles [19]. This process was able to recover nearly 84% of TPA from amorphous PET films as well as a single-use PET bottle following ozonation pretreatment. Therefore, it is imperative to determine the efficacy of such pretreatment for an optimal combination for complete hydrolysis. Even though chemical hydrolysis may be able to recover higher yields of the monomers, processes that operate under near ambient conditions and require no toxic chemicals are preferred.

Biological degradation is a preferred route for its clean, near-ambient conditions and green approach. In the last few decades, scientists have reported numerous enzymes and microorganisms with PET-hydrolyzing ability [20–24]. Functional groups like C=O and –OH increase the wettability or the hydrophilicity of the polymer surface which in turn increases biodegradation [25,

26]. Additionally, factors like adhesion, surface topology, molecular weight, and additives used in the production of the polymer have a significant impact on biodegradation [27]. Pretreatments help modify these intrinsic properties, making PET more accessible for biodegradation.

Pretreatments such as size reduction augment the overall surface area for reaction, while thermal and ultraviolet (UV) pretreatments induce polymer oxidation, subsequently leading to the generation of random radicals [28]. Both thermal and photo-oxidation, increase the incorporation of atmospheric oxygen into the polymer, decreasing the hydrophobicity [28, 29]. The efficacy of UV pretreatment depends on its ability to penetrate through the PET surface since the reaction is a surface phenomenon. Irradiation with UVA with natural weathering conditions resulted in chain scission of PET [30]. Furthermore, Vague et al. [27] reported a change in functional groups after UVA irradiation with no further detail on its effects on biodegradation. Falkenstein et al. [31] also report an impairment in the biodegradation post UV irradiation. Different UV ranges have different energies and hence different penetrative and bond cleavage abilities. Similarly, temperature also affects biodegradation. Temperatures around the glass transition temperatures (amorphous 67 °C and crystalline 81 °C) allow movement of the polymer chains [32, 33]. Most studies exposing PET to heat follow thermal degradation and have not used a method to modify the polymer's physical structure to augment biodegradation. Both the physical and chemical nature of PET affects biodegradation. Sepperumal et al. [34] reported modification of the functional groups of powdered PET after biodegradation with *Penicillium* spps. Furthermore, Farzi et al. [23] reported about 70% biodegradation of PET powder (size 212 µm) by Streptomyces spp. after 18 days. Ma et al. [35], further reduced the size of PET to nanometers and observed biodegradation up to 50%. Most studies of PET pretreatment and biodegradation focus on using one type of pretreatment with one type of biodegradation process. This makes the comparison of such processes difficult. Therefore, a comprehensive study focussing on various pretreatments followed by enzymatic, whole cell, and chemical hydrolyses was carried out to shed some light on the best combination required for PET biodegradation.

This study focuses on the effect of physicochemical treatments of PET for biodegradation using biological catalysts. Eighteen different pretreatments which include acid treatment, thermal oxidation, photooxidation, size reduction, and a combination of thermal oxidation and size reduction were carried out. The effect of pretreatment on the physical and molecular structure of PET was analyzed and subsequently, its impact on biodegradation was analyzed. PET samples were biodegraded using two types of bioagents, whole-cell broths of *Thermobifida fusca* YX and immobilized cutinase enzyme. In addition to biological degradation, the untreated and pretreated PET samples were chemically degraded using non-aqueous alkali.

Materials and methods

Biological agents and chemicals

All experiments were carried out using amorphous PET films purchased from Goodfellow (Canada) (Product code: ES30-FM-000145). The actinomycete, *Thermobifida fusca* (ATCC BA-629), was purchased from Cedarlane (Canada). The immobilized enzyme Novozym® 51,032 (1,3 Lipase from *Humicola insolens*) was purchased from Cedarlane (Canada) (Product code: IMML51-T1-350–2). The immobilized enzyme beads had particle sizes ranging from 300 to 700 µm (immobilized by adsorption onto polymethacrylate divinylbenzene copolymer beads). All the other chemicals and solvents were purchased from Sigma-Aldrich (St. Louis, MO, USA) of reagent grade and used without modification unless specified otherwise.

Physicochemical pretreatments of PET

Ultraviolet (UV) pretreatment

The 2.54×2.54 cm amorphous PET film samples were exposed to two UV wavelengths, 254 nm (UVC) and 311 nm (UVB). The UVC pretreatment used was a modified protocol used by Leggett and Hurley [29]. The sample was kept 3 cm from the UVC light source inside a biosafety cabinet (maximal peak at 254 nm) for 2, 4, and 6 h. The same protocol was used for comparison with the UVB light source using a Philips Narrowband purchased from Philips, Canada.

Size reduction

Amorphous PET was pulverized in an Electric Grain Mill Pulveriser (Rocita, Canada, Model No.: 3558195–1) at 2-min intervals to reduce the effect of heat on the PET particles. The PET particles were separated with mesh sizes 1 mm, 500 µm, and 250 µm. For subsequent experiments, 185 mg of the separated particles were used for each condition evaluated.

Thermal pretreatment of films and size-reduced PET

Amorphous PET film was cut into 2.54×2.54 cm samples and the size-reduced PET samples (1 mm, 500 µm, and 250 µm) were incubated at 70 °C, 80 °C, and 90 °C in a hot air oven, respectively, for 2 weeks.

Acid pretreatment

A modified protocol adapted from Rajandas et al. (2012) was used for the acid pretreatment of PET films. The amorphous PET film was cut into 2.54×2.54 cm samples

and submerged in 10 mL of 65% v/v nitric acid in 25 mL glass bottles with lids for 2 weeks. After every pretreatment, the PET films were washed with 0.1% SDS and subsequently washed three times with distilled water.

Analysis methods

Fourier transform infrared spectrometry (FTIR)

The test film samples were washed thoroughly with deionized water. Spectra were collected in the 4000 to 600 cm^{-1} range at 2 cm^{-1} spectral resolution using a single-beam Bruker Tensor 37 FTIR (Billerica, USA). The instrument had the Bruker OPUS 5.5 software available at the Lakehead University Instrumentation Laboratory (LUIL), Lakehead University, Thunder Bay, Canada.

Differential scanning calorimetry

The untreated and pretreated PET film samples were cut into 2×2 mm squares. Differential scanning calorimetry was carried out in the DSC Q2000 TA Instruments (New Castle, USA) the temperature range was 20 to 270 °C and the heating rate of 10 °C per min. The obtained values were viewed and analyzed using TA Universal Analysis.

The degree of crystallinity (X_C) was calculated according to Eq. (1):

$$X_c = \frac{\triangle H_m - \triangle H_{CC}}{\triangle H_m^0} \times 100 \quad (1)$$

Where ΔH_{cc} is the cold crystallization enthalpy (numerical value) of the sample. ΔH_m is the heat of melting of the sample, while ΔH^0_m is the heat of melting of a pure crystalline sample which is 140 $J.g^{-1}$ according to [37].

Scanning electron microscopy

The untreated and pretreated PET film samples were washed thrice with deionized water and air-dried before imaging. These samples were imaged using the SEM/EDS: Hitachi Su-70 Schottky Field Emission scanning electron microscope (Tokyo, Japan) operated at an electron beam intensity of 5 kV at LUIL, Lakehead University, Thunder Bay, Canada. Before viewing under the microscope, the samples were carbon coated using the BOC Edwards Auto 306 to increase the electron density.

Gravimetric weight loss

The pretreated samples were weighed before and after the pretreatments using the Sartorius Quintix Analytical Balance (Göttingen, Germany). The samples were also weighed before and after biological hydrolysis and chemical hydrolysis.

Biological hydrolysis

Two types of biological hydrolyses, enzyme-mediated and whole-cell-based methods, were employed to determine the efficacy of pretreatment. After the biological hydrolysis, the PET films and particles were separated by vacuum filtration. The PET films and particles were then washed with deionized water three times and were dried at 50 °C in a hot air oven for 6 h and then weighed. Biological hydrolysis was done in triplicates and subsequently subjected to a *t*-test to determine significance.

Enzyme-mediated hydrolysis

The reaction system consisted of 700 mg immobilized Novozym® enzyme (with an activity of 10,000 $\mu mol.g^{-1}.min^{-1}$) (see Supplementary method 1 for determination of enzyme activity) and the pretreated sample in 10 mL of 200 mM Tris HCl buffer at pH 8.0. This system was incubated at 60 ± 2 °C at 150 rpm for 3 days. The enzyme was separated by vacuum filtration, and the PET samples were washed with deionized water thrice before drying in the hot air oven at 50 °C. These samples were then weighed to determine weight loss.

Whole-cell mediated hydrolysis

The actinomycete *T. fusca* YX was grown in 25 mL of Hagerdahl medium (ATCC medium 2382) for 5 days at 150 rpm at 50 °C. The enzyme activity of the extracellular broth was determined to be 28.36 $\mu mol.ml^{-1}.min^{-1}$. The pretreated sample was incubated with 100 µL of *T. fusca* YX inoculum in a Hagerdahl medium for 2 weeks.

Chemical hydrolysis by non-aqueous alkali

Chemical hydrolysis of PET was adapted from Bhogle and Pandit [38]. It was carried out by incubating amorphous PET samples (2.54×2.54 cm) in 20 mL of 8.5% w/w NaOH in methanol in a 125-mL Erlenmeyer flask in a CPX series ultrasonic bath (40 Hz, CAT: 15–337-419), Fisher Scientific (New Hampshire, USA) set at 60 °C for 2.9 h. The reaction was stopped by the addition of an equal volume of chilled deionized water. The unhydrolyzed PET was separated using vacuum filtration, and then washed thrice with deionized water, followed by drying at 80 °C for 45 min to remove any residual methanol. After this, the weight of the unhydrolyzed PET was determined using the Sartorius Quintix weighing balance. The TPA in the filtrate was precipitated at pH 2.5 using undiluted sulphuric acid. The insoluble white precipitate was washed thrice with deionized water to remove soluble salts. The TPA salt was then dried in the hot air oven at 80 °C for 45 min. The TPA yield was calculated using the TPA recovered after precipitation and the theoretical expected TPA. The theoretical calculations for expected TPA were based on the equations from Bhogle and Pandit [38]. The total monomer yield was calculated using the formula in Eq. (2).

$$\text{TPA yield} = \frac{\text{Quantified TPA}}{\text{Theoretical TPA}} \text{ x } 100 \quad (2)$$

where,

Quantified TPA is the number of moles of TPA quantified after hydrolysis.

Theoretical TPA is the number of moles of TPA expected after complete hydrolysis.

Results and discussion

Oxidative degradation

Photo-oxidative degradation using ultraviolet radiation

Most previous studies report weathering of PET by exposure to most of the UV range (400 nm to 250 nm) [31, 39, 40]. In this study, to determine the effect of wavelength and exposure time of UV radiation, PET films were exposed to two specific wavelengths with different energies, 254 nm, and 311 nm. They were irradiated for 3, 4, and 6 h at each wavelength. The surface structure after irradiation remained unchanged when imaged. However, with ATR-FTIR analysis, changes in the intensity of functional groups were observed. Untreated PET samples showed characteristic absorption peaks which include 2864 cm^{-1} and 2945 cm^{-1} for stretching of the asymmetrical/symmetrical C–H bond in a methylene group, 1714 cm^{-1} for C=O stretching in an α/β-unsaturated ester in a benzene ring, 1408 cm^{-1} for stretching of C=C in the benzene ring, 1257 cm^{-1} and 1242 cm^{-1} for stretching of C–O in a carboxylic acid, 1095 cm^{-1} for stretching of C–H bond in the benzene ring, 870 cm^{-1} for bending of C=C in cyclic or conjugated alkene and 725 cm^{-1} for C–H bending in a monosubstituted benzene ring [41–43]. Furthermore, the degree of crystallinity of the untreated PET films, as calculated using Eq. (2), was found to be 6.69%.

For PET samples irradiated with UVB or UVC, a general reduction in peak intensities was observed. UVC irradiation for 3 h caused a decrease in peak intensities, followed by an increase at 4 h, and then a return to the 3-h levels after 6 h. Specifically, the asymmetrical/symmetrical C–H bond in a methylene group at 2945 cm^{-1} and the C=O stretching in an α/β-unsaturated ester at 1714 $cm-^{1}$ showed reductions, indicating bond cleavage near the aromatic moiety (see Fig. 1) [44]. After 4 h, the peak intensities increased, suggesting chain scission and exposure of more functional groups. By 6 h, the intensities decreased again, resembling the 3-h spectrum (see Fig. 2). Photolysis initiated by UV disrupted C–O and C–H bonds at 2945 cm^{-1} and unsaturated sites at 1714 cm^{-1} [28], are evident after 3 h of UVC exposure. Furthermore, differential scanning calorimetry (DSC) analyses of the films subjected to UVB and UVC irradiation revealed a progressive increase in the degree of crystallinity over time. Specifically, the degree of crystallinity for the UVB irradiated samples was determined to be 7.87%, 8.44%, and 10.37% after 3, 4, and 6 h of exposure, respectively (see Supplementary Fig. S1). In comparison, UVC irradiated samples exhibited degrees of crystallinity of 8.83%, 9.07%, and 11.43% following 3, 4, and 6 h of irradiation, respectively (see Supplementary Fig. S2).

Propagation reactions are auto-oxidation cycles which can be observed by the increase after 4 h of irradiation followed by a drop in the peak intensity after 6 h of irradiation. Photolysis occurs through Norrish I and II reactions following the β-scission route. Norrish reactions in polyesters like PET commence with the formation of an excited terephthalic acid radical [41, 45, 46]. Due to

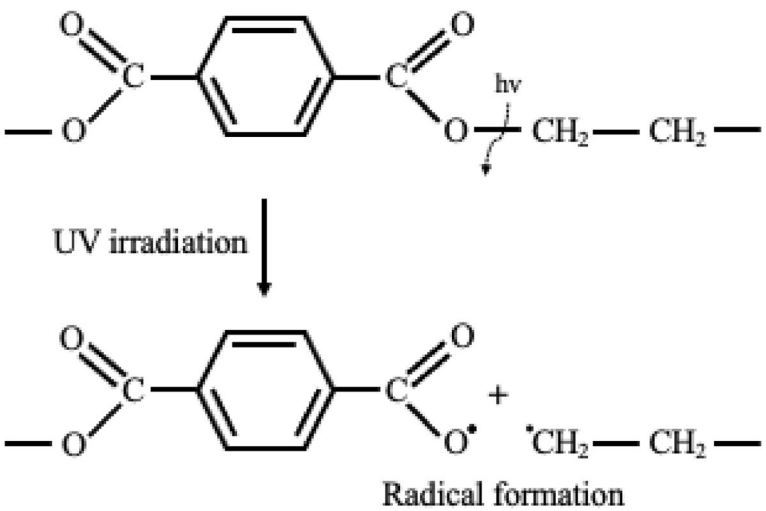

Fig. 1 Schematic of the postulated photodegradation process as a result of UV irradiation

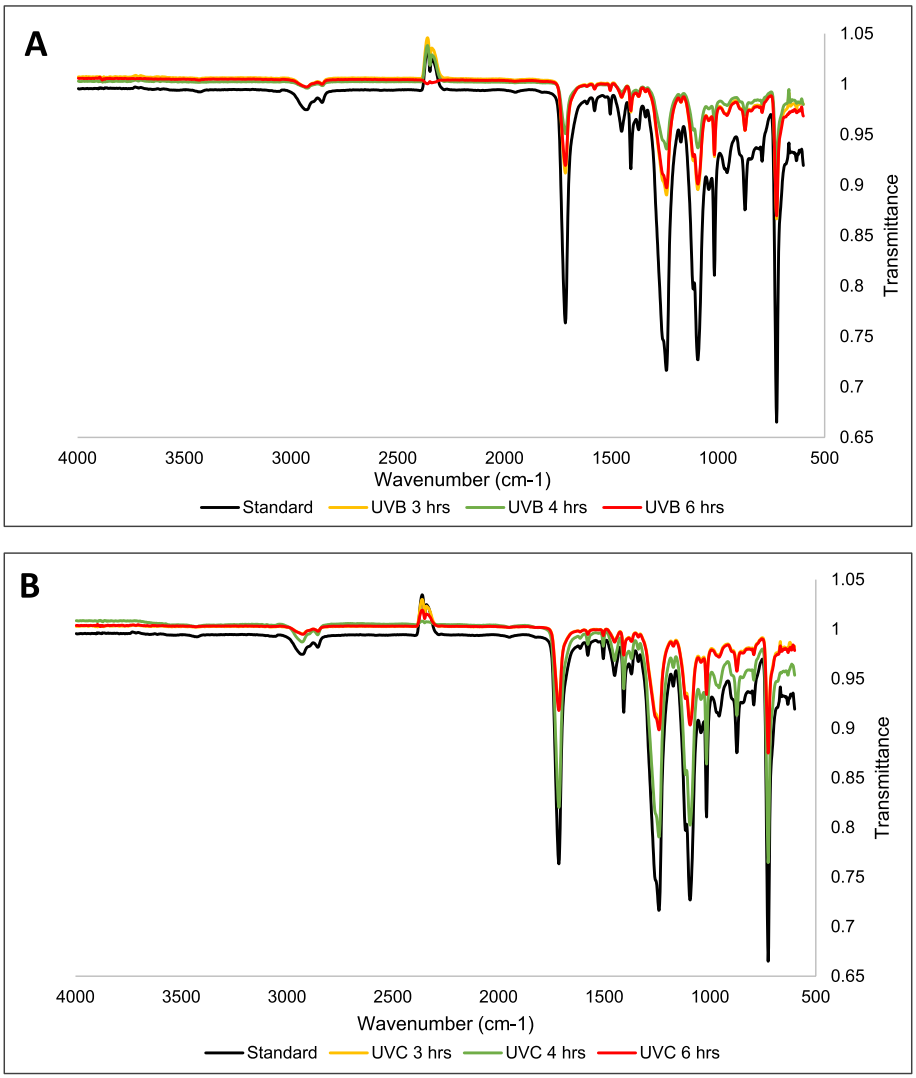

Fig. 2 ATR-FTIR spectra of amorphous PET films exposed to **A** UVB and **B** UVC for 3, 4, and 6 h versus untreated PET

the domination of type I reaction, carbonyl bonds are cleaved. These scissions occur in the amorphous domain creating two free ends that can restructure to increase the crystallinity of the polymer. The results obtained in this study with UV photolysis pretreatment are similar to those described previously by Singh and Sharma [28]. Irradiation with shorter wavelengths like 254 nm is known to reduce the molecular weight of PET, while 310 nm has a much-reduced extent of molecular weight reduction. Reduced molecular weight polymers can restructure with ease compared to their larger counterparts [39].

Following UV irradiation, the efficacy of biodegradation was assessed. There was an increase in *T. fusca*-mediated biodegradation with UVB-irradiated PET films. PET films irradiated with UVB for 6 h demonstrated nearly a 4% weight loss compared to the untreated PET sample at 1%. In comparison, enzyme-mediated biodegradation showed a 15% decrease compared to its untreated PET counterpart after 3 h of UVB irradiation. With UVC irradiation, there was a decrease in the biodegradation performance with both enzyme-mediated, HiC, and whole-cell *T. fusca* biodegradation (see Fig. 3). Falkenstein et al. found that weathering of PET for 14 days with a focus on UV exposure resulted in an increase in the abundance of C–O bonds due to intrachain scissions [31]. However, this was accompanied by a decrease in the biodegradation efficiency. This was attributed to the increase in the crystallinity of the PET film after irradiation. In this study, a narrower range of

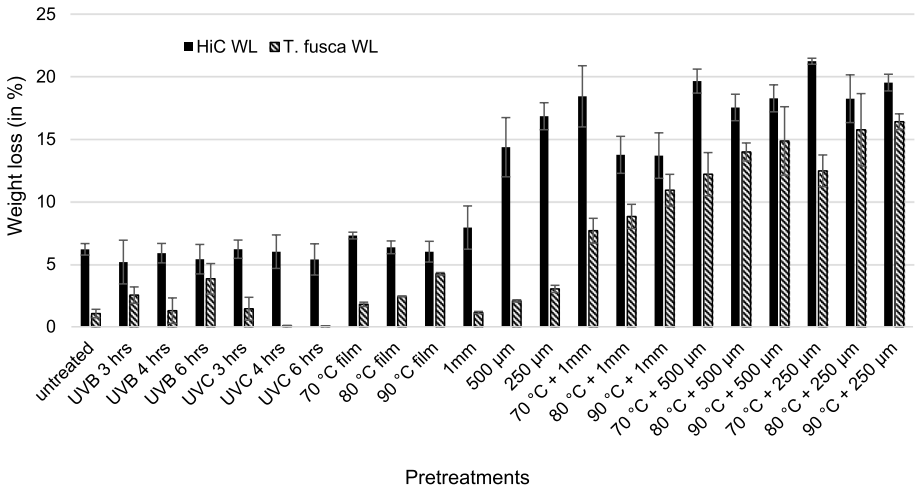

Fig. 3 Weight loss of PET based on enzymatic biodegradation by immobilized HiC and whole-cell biodegradation by *Thermobifida fusca* YX following pretreatment by UVB and UVC irradiation, thermal oxidation, size reduction, and thermal oxidation of size-reduced particles

wavelengths with peak intensities of 311 nm (UVB), and 254 nm (UVC) with shorter time exposures resulted in no new peaks, but a variation in the abundance of C=O and C–H which corroborates the findings of Falkenstein et al. Suggesting that the effects of UV exposure on PET films are demonstrated in 4 h. This indicates that the 4-h mark of UVC exposure is the critical time point beyond which impairment of biodegradation occurs. Hence, UVC exposure of more than 4 h would not be a recommended pretreatment method.

Thermal oxidation

Thermal oxidation was assessed by exposing the PET film to dry heat at three temperatures, 70 °C, 80 °C, and 90 °C for 2 weeks. With each increase in temperature, there was a corresponding increase in the haziness of the films. Haze can be caused due to surface roughness, internal optical irregularities, level of crystallization, and porosity [47, 48]. At higher temperatures, the polymer chains can shift freely enough to be able to form crystals. DSC analysis of the treated films revealed a temperature-dependent increase in crystallinity. This was substantiated by the observed degrees of crystallinity at temperatures of 70 °C, 80 °C, and 90 °C, which were measured to be 7.23%, 7.35%, and 7.51%, respectively (see Supplementary Fig. S3). The effects of thermal treatment on the surface of the films were imaged using a scanning electron microscope. Multiple physical deformities like bulbous protrusions and cracks of varying widths were present on the film's surface. These deformities increased in frequency and intensity with an increase in temperature (see Supplementary Fig. S4).

There were no shifts in the hybridization state or electron distribution of the molecular groups within the fingerprint region when observed by ATR-FTIR. However, there was a variation in the abundance of the functional groups as indicated by a change in the peak intensity [49]. There was a slight increase in the stretching in the asymmetrical C–H bond at 2945 cm^{-1} when the PET films were exposed to 70 °C and 80 °C for 2 weeks. Meanwhile, there was a decrease when exposed to 90 °C for 2 weeks (see Fig. 4). We observed a shift in the paradigm when exposed to 90 °C. This suggests a reduction in the C–H bonds upon an increase in temperature from 80 to 90 °C, which corresponds to the reduction in the bond between the asymmetrical C-atoms on either side of the aromatic ring with their corresponding H-atoms. This can be further confirmed by the reduction in the peak intensity at 1714.64 cm^{-1} which corresponds to the stretching of the bond between the C=O of an α/β-unsaturated ester in a benzene ring. This strongly indicates the cleavage of the bond or bonds between the asymmetrical carbons and the respective substitutions. Correspondingly, at peak 1714.64 cm^{-1} we observed a progressive increase in the stretching of C=O up to 80 °C but observed a decrease when the temperature is increased to 90 °C. Thermal oxidation, similar to photo-oxidation follows similar initiation and propagation reactions [28]. Additionally, the thermal oxidation of PET and its structural homolog, ethylene dibenzoate resulted in a radical formation across C–O in the ester bond [32]. These results suggest that the initiation of thermal oxidation can occur with temperatures close to the glass transition temperature, that is as low as 70 °C.

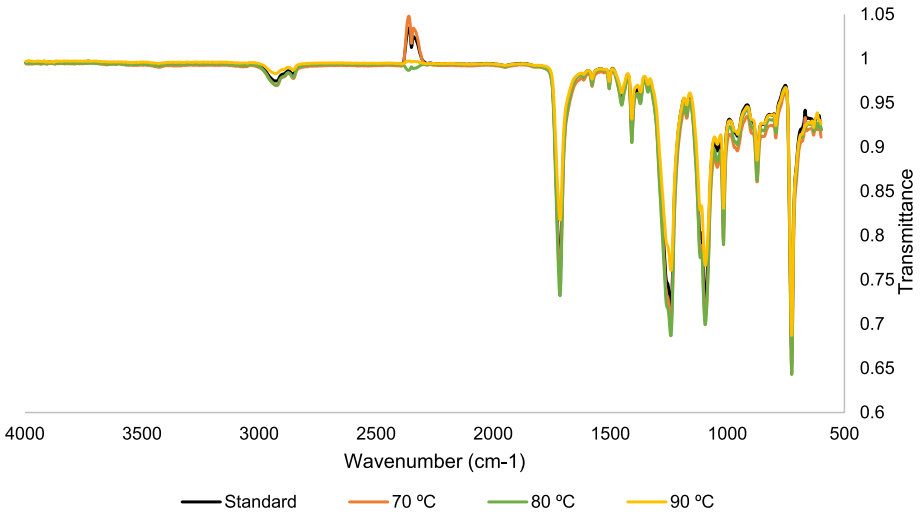

Fig. 4 ATR-FTIR spectra of amorphous PET film exposed to exposed to 70 °C, 80 °C, and 90 °C for 2 weeks versus untreated PET

The effect of 90 °C was observed when the thermally treated samples were subjected to biodegradation. With both, the immobilized HiC and the whole-cell *T. fusca* there was a decrease in the weight loss compared to the untreated PET film (see Fig. 3). The increase in temperature above the glass transition temperature permits the movement of polymer chains which allows the formation of more crystalline regions. Biodegradation of thermally treated PET films with immobilized HiC and whole-cell *T. fusca* yielded contrasting results. PET films exposed to 70 °C resulted in 7.3 ± 0.27% weight loss with the immobilized enzyme HiC, which is a minimal increase compared to the untreated PET film. Further increase in the pretreatment temperature (90 °C) impaired the biodegradation resulting in a decrease in weight loss with immobilized HiC. In contrast, there was a proportional increase in weight loss with an increase in temperature when biodegraded with whole-cell *T. fusca*. Like cellulases, *T. fusca* YX could harbor multiple active PET-hydrolyzing enzymes as well as modifying enzymes that resulted in higher weight loss. This could contribute towards the increase in biodegradation of PET which has been thermally oxidized at 90 °C. Although the biodegradation of *T. fusca* YX increases with temperature, the energy consumption associated with a 2-week thermal treatment is disproportionate to the observed biodegradation. While the method shows potential, its viability requires further evaluation through a comprehensive life cycle analysis.

Size-reduction

In order to determine the effect of particle size, PET samples were pulverized to 1 mm, 500 µm, and 250 µm. When imaged, the structure of the cross-sectional surface showed rough edges and several cracks resulting from pulverizing. In some cases, bulbous protrusions could be observed (see Supplementary Fig. S5). Similar to the effect of thermal oxidation, there were no changes in the particles' hybridization states or functional groups, but there were variations in the abundance of the functional groups. A slight shift in peaks is observed upon size reduction compared to the standard PET film. Particle size 1 mm shows a peak shift to 2949 cm^{-1}, while 500 µm and 250 µm show a shift to 2927 cm^{-1} (see Supplementary Fig. 6). These shifts still fall in the methyl C–H asymmetrical stretch. Furthermore, with a progressive increase in size, there is a corresponding increase in the peak intensities. This confirms the increase in the exposure of functional groups due to the increase in surface area.

Previous reports demonstrate an inverse correlation between particle size and biodegradation, i.e., a decrease in particle size has increased biodegradation [23]. Both enzyme-mediated and whole-cell-mediated biodegradation showed a similar trend of increase in overall weight loss with a decrease in particle size. Weight loss was more substantial with HiC-mediated biodegradation compared to *T. fusca*-mediated biodegradation. With HiC-mediated biodegradation, the highest weight loss of 16.85 ± 1.08% (absolute weight loss of 33.26 ± 1.96 mg) was observed with the smallest particle size, 250 µm. This is 2.7 times more than the weight loss observed with untreated PET films, 6.2 ± 0.46% (absolute weight loss of 13 ± 0.5 mg) after 3 days of enzymatic hydrolysis. Furthermore, with whole-cell mediated biodegradation, there was a three times increase in biodegradation (3.03 ± 0.5% weight loss) with 250 µm particles than with untreated PET films. The reduction in particle size increases the surface area available per unit mass for reaction increasing reaction rates.

However, the energy input for the size reduction and the ability to bring about size reduction at higher volumes needs to be studied as at a large scale this cost can be prohibitive.

Combination of thermal oxidation with size-reduction

As observed, reduction in particle size and thermally oxidized PET increases the overall biodegradation. To assess the combined effect, sized-reduced PET particle sizes, 1 mm, 500 µm, and 250 µm were thermally treated at three temperatures 70 °C, 80 °C, and 90 °C for 2 weeks. When imaged, all samples were observed to have an increased number of fine cracks throughout the surface. In addition, several broken-like structures were found toward the particles' sides. With an increase in temperature, various undulating protrusions were observed on the particle's surface compared to the untreated film (see Supplementary Figs. S7–S9).

After the assessment of changes in the physical structure, the changes in the molecular bonds and functional groups were assessed. The variation in functional groups resulting from the combination of thermal oxidation and size reduction pretreatments was assessed using ATR-FTIR. The combination of size reduction and temperature resulted in the variation of peak intensities following the thermally affected peaks, 2945 cm^{-1} and 1714 cm^{-1}. The peak at 2945 cm^{-1} corresponds to the stretching of the asymmetrical methyl C–H bond on either side of the aromatic ring and the peak at 1714 cm^{-1} corresponds to the stretching of the bond between the C = O of an α/β-unsaturated ester in a benzene ring respectively (see Supplementary Fig. S10). The combination of size reduction with exposure to 70 °C has increased overall peak intensities when compared to their corresponding controls of unheated size-reduced particles. An increase in the functional groups has been previously reported to be conducive to biological hydrolysis [36]. This was confirmed in our study, where the combination of 250-size particles treated at 70 °C for 2 weeks resulted in the highest weight loss of 21.25 ± 0.24%. When exposed to 80 °C for 2 weeks, interestingly, there was both an increase and decrease in peak intensities at different wavelengths. With a decrease in size up to 500 µm, there was a decrease in peak intensities. With further decrease in size to 250 µm, there was an increase in peak intensities. This suggests an increase in the stretching of the C–H bond corresponding to the increase in abundance of the methylene group. The increase in the abundance of functional groups in the sample with a particle size of 250 µm was due to the increased surface area. These results suggest the increase in bond cleavage with an incremental decrease in size resulting in an increase in the abundance of functional groups C = O and C–H. When combined with even increased temperature, 90 °C there was a further reduction in the peak intensity. Following the earlier mentioned peaks, 2945 cm^{-1} and 1714 cm^{-1}, similar bond cleavage can be observed. The reduction in the asymmetrical C-bond on either side of the aromatic ring is indicative of its cleavage and the reduction in the stretching of the bond between the C = O of an α/β-unsaturated ester in a benzene ring which is indicative of the cleavage of the bond. There seemed to be a greater effect of bond cleavage with 250 µm exposed to 90 °C.

As mentioned earlier, size reduction and thermal treatment confer unique properties to the previously smooth polymer. Size reduction increases the overall surface area, roughness, and exposure of functional groups due to the pulverizing process. Depending on the temperature there can either be an increase (at 70 °C and 80 °C) or a decrease (at 90 °C) in the abundance of functional groups. The combination of these treatments resulted in both physical and chemical changes in PET, which augmented biodegradation. The combination of different sizes with different temperatures did not result in a synergistic effect for enzyme-mediated hydrolysis. However, there was an increase in weight loss compared to their non-temperature-treated counterparts. The highest weight loss with whole cell mediated hydrolysis was 16.41 ± 0.63% with 250 µm particles treated at 90 °C. As mentioned earlier, *T. fusca* YX could have a battery of PET-hydrolyzing enzymes (PHEs) as well as modifying enzymes. Meanwhile, the highest weight loss with immobilized enzyme was 21.25 ± 0.24% with 250 µm particles treated at 70 °C. Our results suggest that immobilized HiC is a better option for biodegradation of size-reduced PET particles. However, there was a synergistic effect of the combination of size reduction and temperature with whole-cell mediated biodegradation with uninduced *T. fusca* YX. Induction of cutinases from *T. fusca* YX could potentially increase the overall biodegradation of PET particles.

The reduction of PET particle size presents inherent challenges, including the risk of microplastic and nanoplastic release into the environment [3] and the substantial energy required for the size reduction process. Additionally, thermal treatment for 2 weeks would further increase energy consumption. However, the significant weight loss observed through both whole-cell and immobilized enzymatic biodegradation highlights the potential of the biological method. Optimizing the process to minimize energy consumption, followed by a comprehensive life cycle analysis, could provide valuable insights into the feasibility and sustainability of this approach.

Acid pretreatment

PET films were treated with 65% v/v nitric acid to assess the effect of strong acid on the polyester. After 2 weeks, the films had turned completely white and were extremely brittle to handle. When viewed under the electron microscope, the surface of the films was completely deteriorated. There were craters and tiny holes throughout the surface of the film (see Supplementary Fig. S11). Despite the visual indication of deterioration of the film, interestingly, the weight of the film increased by 5.73 ± 0.71% after the acid treatment. The assessment of functional groups by ATR-FTIR determined a change in the functional groups present, there was an additional broad peak ranging from 3206 cm^{-1} to 3583 cm^{-1} which suggests the presence of an –OH bond. Meanwhile, the other peaks remained unchanged (see Supplementary Fig. S12). The drastic change in the physical structure and the formation of a new functional group did not augment biodegradation. In fact, there was no change in weight after enzymatic hydrolysis with HiC, indicating that no biodegradation occurred. With whole-cell hydrolysis, there was 5.68 ± 0.38% weight loss. This suggests that different enzymes were expressed by *T. fusca* that had a different cleavage mechanism than HiC. The actinomycete has been previously described as having a battery of enzymes for cellulolytic activity [50] and is currently being explored for other functions, like esterase activity. Additionally, the variation in the physical states of HiC (immobilized) and the whole cells (free suspension) could have affected the biodegradation.

Chemical hydrolysis by non-aqueous alkali

Chemical hydrolysis involving non-aqueous alkalis has been gaining interest due to its ability to hydrolyze in-use plastic that would otherwise end up in landfills. Recent studies report the use of standard PET films as well as waste PET able to be hydrolyzed with non-aqueous alkali. One such study reports the chemical breakdown of amorphous untreated PET films results in over 80% TPA recovery [19]. As observed earlier in this study, pretreatments cause chemical and, in some cases, physical changes. To determine the effect of pretreatment on TPA yield, each sample was exposed to individual and combined pretreatments prior to being chemically hydrolyzed using 8.5% NaOH in methanol in combination with ultrasonic waves for 2.9 h. Under these conditions, all PET samples had a 100% weight loss. Untreated PET sample resulted in as high as 90.85 ± 0.84% TPA recovered (using Eq. (2)). As demonstrated by a previous study, HPLC analysis of the supernatant after the precipitation of TPA revealed trace amounts of TPA, MHET, BHET, and other oligomers [19]. There was no significant difference between the TPA yields between the untreated film and pretreated samples (see Fig. 5). Due to the caustic nature of the treatment, no pretreatment would be required.

Conclusion

This study aimed to identify the physicochemical changes in amorphous PET films on pretreatment and their ability to augment biodegradation. Pre-treatments like thermal oxidation with dry heat and photooxidation by UV irradiation targeted C=O and C–H bonds. Despite targeting

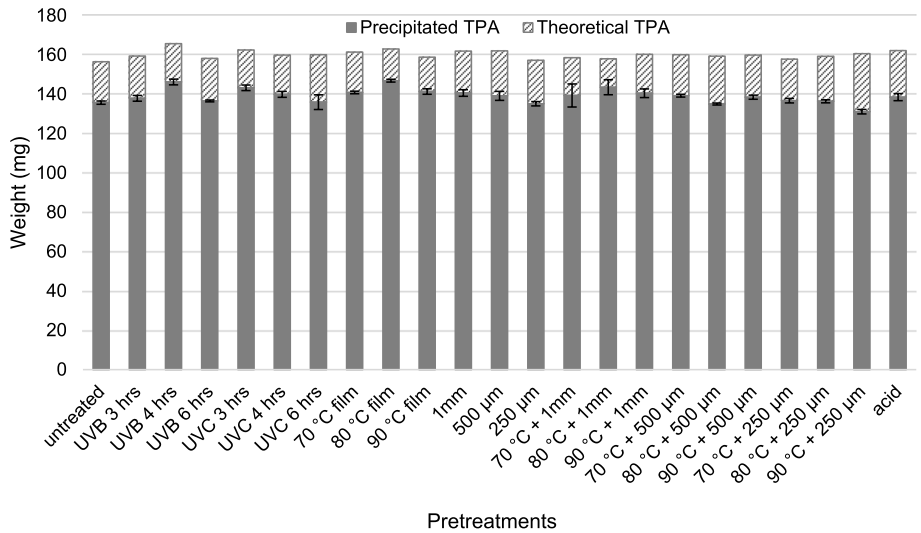

Fig. 5 Visualization of the weight (in mg) of terephthalate (TPA) precipitated after chemical hydrolysis from the predicted theoretical TPA (based on complete depolymerization of PET)

the same bonds, UV irradiation impaired biodegradation while thermal oxidation increased biodegradation. Interestingly, *T. fusca*-mediated biodegradation was better than a singular enzyme, HiC, when PET was exposed to higher temperatures like 90 °C. While acid pretreatment demonstrated a change in the hybridization state of the functional groups, i.e., an additional alcohol (–OH) peak was observed. Despite the severe nature of the acid pretreatment, no large increase in biodegradation was observed compared to the other pretreatments. Size reduction produced the highest biodegradation and can be attributed to the increased surface area of PET. The combination with the highest weight loss, 21.25 ± 0.24% was with the smallest particle size, 250 µm at 80 °C with the immobilized HiC enzyme. However, this process is not only energy intensive but could also lead to the generation of microplastics that could potentially enter the environment. These results suggest that whole-cell biodegradation is not just dependent on the shift in the hybridization peaks but also its abundance. Biodegradation is thus affected by the size of the particle, exposure to shorter wavelengths like UV, and thermal treatments closer to glass transition temperatures. Commercial PET films with increased crystallinity (20–30%) may exhibit behavior distinct from or analogous to the effects observed in the pretreatments discussed in this study, albeit at a different magnitude. This elevated crystallinity could potentially lead to a reduction in the biodegradation efficiency typically observed with amorphous PET, as the denser crystalline structure may further limit enzymatic or microbial access to the polymer chains. Biodegradation requires modification of PET via physicochemical pretreatments while chemical hydrolysis does not require any pretreatment. The caustic nature of the chemical process overcomes the need for any modification. Further life cycle assessments of the described physicochemical and biodegradation methods need to be studied to identify the most optimal route for reduction in pollution under milder conditions like biological reactions that can lead to a circular economy.

Supplementary Information

The online version contains supplementary material available at https://doi.org/10.1186/s44314-025-00018-5.

Supplementary Material 1: Supplementary Method 1. Analysis of esterase activity by para-nitrophenyl butyric acid (pNPB) hydrolysis assay. Esterase activity was quantified using pNPB (10 µL of 10 mM) as the substrate in 1 mL of 200 mM Tris–Cl (pH 8.0). The reaction was started by the addition of 100 µL of supernatant and incubated at 60 ℃ for 8 min. The generation of para-nitrophenol was quantified at 405 nm using the xMark™ Microplate Absorbance Spectrophotometer, Bio-Rad Laboratories Inc. Enzyme concentration was determined by measuring absorbance at 280 nm. Supplementary Figure S1. Differential scanning calorimetric analysis of untreated PET (black) and UVB irradiated PET (3 h (orange), 4 h (green), 6 h (blue)). Supplementary Figure S2. Differential scanning calorimetric analysis of untreated PET (black) and UVC irradiated PET (3 h (orange), 4 h (green), 6 h (blue)). Supplementary Figure S3. Differential scanning calorimetric analysis of untreated PET (black) and thermally treated PET (70 °C (orange), 80 °C (green), and 90 °C (blue)). Supplementary Figure S4. Scanning electron images of amorphous PET films exposed to (A) 70 °C, (B) 80 °C, and (C) 90 °C for two weeks. Image of untreated PET film (D). Supplementary Figure S5. Scanning electron images of PET particles at sizes (A) 1 mm, (B) 500 µm, and (C) 250 µm. Image of untreated PET film (D). Supplementary Figure S6. FTIR spectra of PET particles at sizes 1 mm (orange), 500 µm (yellow), and 250 µm (green) versus untreated PET spectra (black). Supplementary Figure S7. Scanning electron images of PET particles at sizes (A) 1 mm, (B) 500 µm, and (C) 250 µm pretreated at 70 °C for two weeks. Image of untreated PET film (D). Supplementary Figure S8. Scanning electron images of PET particles at sizes (A) 1 mm, (B) 500 µm, and (C) 250 µm pretreated at 80 °C for two weeks. Image of untreated PET film (D). Supplementary Figure S9. Scanning electron images of PET particles at sizes (A) 1 mm, (B) 500 µm, and (C) 250 µm pretreated at 90 °C for two weeks. Image of untreated PET film (D). Supplementary Figure S10. ATR-FTIR spectra of size reduced particles thermally treated at (A) 70 °C, (B) 80 °C, and (C) 90 °C for two weeks. Untreated PET particles are depicted as follows: 1 mm (green), 500 µm (yellow), and 250 µm (red). (A) FTIR spectra of PET particles at sizes 1 mm (dark green), 500 µm (orange), and 250 µm (dark red) exposed to 70 °C for two weeks versus their corresponding untreated samples. (B) FTIR spectra of PET particles at sizes 1 mm (dark green), 500 µm (orange), and 250 µm (dark red) exposed to 80 °C for two weeks versus their corresponding untreated samples. (C) FTIR spectra of PET particles at sizes 1 mm (dark green), 500 µm (orange), and 250 µm (dark red) exposed to 90 °C for two weeks versus their corresponding untreated samples. Supplementary Figure S11. Scanning electron images of PET films treated with (A) acid and (B) image of untreated PET film. Supplementary Figure S12. FTIR spectra of acid treated PET film (red) versus untreated PET spectra (black).

Acknowledgements
The authors would like to acknowledge Dr. Gousheng Wu for sample preparation and assistance with the scanning electron microscope, and Michael Sorokopud for assistance with the ATR-FTIR at LUIL, Lakehead University, Thunder Bay. The authors would also like to thank Dr. Pedram Fatehi for providing access to the DSC, and Juan Paez for assistance with DSC at GPRC, Lakehead University, Thunder Bay. Lastly, the authors would like to acknowledge Dr. Brenda Magajna for reviewing and editing the manuscript.

Authors' contributions
R. A: Conceptualization, literature search, methodology, investigation, original draft preparation, review, and editing. S. K. R.: Conceptualization, review and editing.

Funding
The authors acknowledge the support received from the Canada Research Chair Program (CRC).

Data availability
No datasets were generated or analysed during the current study.

Declarations

Competing interests
The authors declare no competing interests.

Author details
[1]Science and Environmental Studies, Lakehead University, Thunder Bay, ON, Canada. [2]Biorefining Research Institute (BRI), Lakehead University, Thunder Bay, ON, Canada. [3]Department of Chemical Engineering, Lakehead University, Thunder Bay, ON, Canada.

Received: 24 September 2024 Accepted: 30 January 2025
Published online: 10 February 2025

References

1. Nisticò R. Polyethylene terephthalate (PET) in the packaging industry. Polym Test. 2020;1(90): 106707.
2. Webb HK, Arnott J, Crawford RJ, Ivanova EP. Plastic degradation and its environmental implications with special reference to poly(ethylene terephthalate). Polymers. 2013;5:1–18. Available from: https://www.mdpi.com/2073-4360/5/1/1/htm. 2012 Dec 28 [cited 2024 Jul 15] .
3. Amanna R, Samavi M, Rakshit SK. Biological degradation of microplastics and nanoplastics in water and wastewater. Curr Dev Biotechnol Bioeng. 2023;1:293–314.
4. PlasticsEurope (PEMRG). In Statista. 2021 [cited 2022 Feb 23]. Annual production of plastics worldwide from 1950 to 2020 (in million metric tons). Available from: https://www-statista-com.ezproxy.lakeheadu.ca/statistics/282732/global-production-of-plastics-since-1950/.
5. Canada Plastics Pact. Canada-wide plastic packaging flows: a progress report [Internet]. 2024. Available from: www.plasticspact.ca.
6. Gourmelon G. Global Plastic Production Rises, Recycling Lags. 2015. Retrieved on 2016:16–2.
7. Amanna R, Mahal Z, Vieira ECS, Samavi M, Rakshit S. Plastics: Toward a Circular Bioeconomy. In: Biomass, Biofuels, Biochemicals. Elsevier; 2021:781–811.
8. Walker TR. (Micro)plastics and the UN sustainable development goals, current opinion in green and sustainable chemistry. 2021;30:100497.
9. Koshti R, Mehta L, Samarth N. Biological recycling of polyethylene terephthalate: a mini-review. Vol. 26, Journal of Polymers and the Environment. Springer New York LLC; 2018. p. 3520–9.
10. Wu WM, Yang J, Criddle CS. Microplastics pollution and reduction strategies. Front Environ Sci Eng. 2017;11:1–4.
11. Paul MB, Stock V, Cara-Carmona J, Lisicki E, Shopova S, Fessard V, et al. Micro- And nanoplastics-current state of knowledge with the focus on oral uptake and toxicity. Nanoscale Adv Royal Soc Chem. 2020;2:4350–67.
12. Revel M, Châtel A, Mouneyrac C. Micro(nano)plastics: A threat to human health?. Current Opinion in Environmental Science and Health. Elsevier B.V.; 2018.;1:17–23.
13. Shen M, Zhang Y, Zhu Y, Song B, Zeng G, Hu D, et al. Recent advances in toxicological research of nanoplastics in the environment: A review. Environmental Pollution. Elsevier Ltd; 2019;252:511–21.
14. Ian Tiseo. Plastic waste worldwide - statistics & facts [Internet]. 2023 [cited 2023 Feb 19]. Available from: https://www.statista.com/topics/5401/global-plastic-waste/#topicOverview.
15. Thoden van Velzen EU, Brouwer MT, Stärker C, Welle F. Effect of recycled content and rPET quality on the properties of PET bottles, part II: Migration. Packaging Technology and Science. 2020;33(9):359–71. [cited 2023 Feb 19]. Available from: https://onlinelibrary.wiley.com/doi/full/10.1002/pts.2528.
16. Welle F. A new method for the prediction of diffusion coefficients in poly(ethylene terephthalate). J Appl Polym Sci. 2013;129(4):1845–51.
17. Brouwer MT, Alvarado Chacon F, Thoden van Velzen EU. Effect of recycled content and rPET quality on the properties of PET bottles, part III: Modelling of repetitive recycling. Packaging Technology and Science. 2020;33(9):373–83.
18. Welle F. Twenty years of PET bottle to bottle recycling - an overview. Resour Conserv Recycl. 2011;55(11):865–75.
19. Moges B. Chemical De-polymerization for reuse of Polyethylene Terephthalate (PET) towards a circular economy. 2022;
20. Maheswaran B, Al-Ansari M, Al-Humaid L, Sebastin Raj J, Kim W, Karmegam N, et al. In vivo degradation of polyethylene terephthalate using microbial isolates from plastic polluted environment. Chemosphere. 2023;1(310): 136757.
21. Torena P, Alvarez-Cuenca M, Reza M. Biodegradation of polyethylene terephthalate microplastics by bacterial communities from activated sludge. Can J Chem Eng [Internet]. 2021 Oct 1 [cited 2023 Feb 17];99(S1):S69–82. Available from: https://onlinelibrary.wiley.com/doi/full/10.1002/cjce.24015.
22. Huang QS, Yan ZF, Chen XQ, Du YY, Li J, Liu ZZ, et al. Accelerated biodegradation of polyethylene terephthalate by Thermobifida fusca cutinase mediated by Stenotrophomonas pavanii. Sci Total Environ. 2022;20(808): 152107.
23. Farzi A, Dehnad A, Fotouhi AF. Biodegradation of polyethylene terephthalate waste using Streptomyces species and kinetic modeling of the process. Biocatal Agric Biotechnol. 2019;1(17):25–31.
24. Qi X, Yan W, Cao Z, Ding M, Yuan Y. Current advances in the biodegradation and bioconversion of polyethylene terephthalate. Microorganisms. 2021;10(1):39.
25. Benke A, Sonnenberg J, Oelschlägel K, Schneider M, Lux M, Potthoff A. Wettability after Artificial and Natural Weathering of Polyethylene Terephthalate. Environments 2022;9(11):134. [cited 2024 Nov 9]. Available from: https://www.mdpi.com/2076-3298/9/11/134/htm.
26. Donelli I, Freddi G, Nierstrasz VA, Taddei P. Surface structure and properties of poly-(ethylene terephthalate) hydrolyzed by alkali and cutinase. Polym Degrad Stab. 2010;95(9):1542–50.
27. Vague M, Chan G, Roberts C, Swartz N, Mellies J. Pseudomonas isolates degrade and form biofilms on polyethylene terephthalate (PET) plastic. BioRxiv. 2019:647321.
28. Singh B, Sharma N. Mechanistic implications of plastic degradation. Vol. 93, Polymer Degradation and Stability. 2008. p. 561–84.
29. Hurley CR, Leggett GJ. Quantitative investigation of the photodegradation of polyethylene terephthalate film by friction force microscopy, contact-angle goniometry, and X-ray photoelectron spectroscopy. ACS Appl Mater Interfaces. 2009;1(8):1688–97.
30. Gok A, Fagerholm CL, Gordon DA, Bruckman LS, French RH. Degradation of poly(ethylene-terephthalate) under accelerated weathering exposures. In: 2015 IEEE 42nd Photovoltaic Specialist Conference, PVSC 2015. Institute of Electrical and Electronics Engineers Inc.; 2015.
31. Falkenstein P, Gräsing D, Bielytskyi P, Zimmermann W, Matysik J, Wei R, et al. UV Pretreatment impairs the enzymatic degradation of polyethylene terephthalate. Front Microbiol. 2020;28:11.
32. Botelho G, Queiro´squeiro´s A, Liberal S, Gijsman P. Studies on thermal and thermo-oxidative degradation of poly(ethylene terephthalate) and poly(butylene terephthalate). Polym Degrad Stab. 2001;74(1):39–48. Available from: www.elsevier.com/locate/polydegstab.
33. Panowicz R, Konarzewski M, Durejko T, Szala M, Łazińska M, Czerwińska M, et al. Properties of polyethylene terephthalate (PET) after thermo-oxidative aging. Materials 2021;14:3833. Available from: https://www.mdpi.com/1996-1944/14/14/3833/htm. [cited 2024 Jan 22].
34. Umamaheswari S, Sepperumal U, Markandan M, Palraja I. Micromorphological and chemical changes during biodegradation of Polyethylene terephthalate (PET) by Penicillium sp [Internet]. Vol. 3, Journal of Microbiology and Biotechnology Research Scholars Research Library J. Microbiol. Biotech. Res. 2013. Available from: http://scholarsresearchlibrary.com/archive.html.
35. Ma M, Wang L, Zhu H. Enzymatic degradation of polyester-nanoparticles by lipases and adsorption of lipases on the polyester-nanoparticles. In: Advanced Materials Research. 2012. p. 2302–7.
36. Rajandas H, Parimannan S, Sathasivam K, Ravichandran M, Su YL. A novel FTIR-ATR spectroscopy based technique for the estimation of low-density polyethylene biodegradation. Polym Test. 2012;31(8):1094–9.
37. Mehta A, Gaur U, Wunderlich B. Equilibrium melting parameters of poly(ethylene Terephthalate). J Polym Sci Polym Phys Ed. 1978;2:289–96.
38. Bhogle CS, Pandit AB. Ultrasound-assisted alkaline hydrolysis of waste poly(ethylene terephthalate) in aqueous and non-aqueous media at low temperature. Indian Chem Eng. 2018;60(2):122–40.
39. Day M, Wiles DM. Photochemical degradation of poly (ethylene Terephthalate). II. Effect of Wavelength and Environment on the Decomposition Process. J Appl Polym Sci. 1972;16(1):191–202.
40. Day M, Wiles DM. Photochemical degradation of poly(ethylene terephthalate). I. Irradiation Experiments with the Xenon and Carbon Arc. J Appl Polym Sci. 1972;16(1):175–89.
41. Zhu Z, Kelley MJ. IR spectroscopic investigation of the effect of deep UV irradiation on PET films. 2005. Available from: www.elsevier.com/locate/polymer. [cited 2023 Feb 27].
42. Huang Y, Shang C, Li L. Novel N-doped graphene enhanced ultrafiltration nano-porous polyvinylidene fluoride membrane with high permeability and stability for water treatment. Sep Purif Technol. 2021;15:267.
43. Alzuhairi M, Al-Ghaban A. Chemical recycling of polyethylene terephthalate (PET) as additive for asphalt [Internet]. 2016. Available from: https://www.researchgate.net/publication/309420408.
44. Smith BC. Infrared spectroscopy of polymers, VIII: Polyesters and the Rule of Three. Spectroscopy (Santa Monica). 2022;37(10):25–8.
45. Fechine GJM, Rabello MS, Souto Maior RM, Catalani LH. Surface characterization of photodegraded poly(ethylene terephthalate) The effect of ultraviolet absorbers. Polymer (Guildf). 2004;45(7):2303–8.

46. DeCosta DP, Bennett AK, Pincock JA. The Norrish Type II photofragmentation of esters induced by intramolecular electron transfer. J Am Chem Soc. 1999;121(15):3785–6. https://doi.org/10.1021/ja9840347. [cited 2024 Nov 24].
47. Horváth Z, Menyhárd A, Doshev P, Gahleitner M, Vörös G, Varga J, et al. Effect of the molecular structure of the polymer and nucleation on the optical properties of polypropylene homo-and copolymers. ACS Appl Mater Interfaces. 2014;6(10):7456–63. Available from: https://pubs.acs.org/doi/full/10.1021/am5008535. [cited 2023 Feb 19]
48. Molnár J, Sepsi Ö, Erdei G, Lenk S, Ujhelyi F, Menyhárd A. Modeling of light scattering and haze in semicrystalline polymers. Journal of Polymer Science. 2020;58(13):1787–95. Available from: https://onlinelibrary.wiley.com/doi/full/10.1002/pol.20200027. [cited 2023 Feb 19].
49. Norman Jones R, Ramsay DA, Keir DS, Dobriner K. The intensities of carbonyl bands in the infrared spectra of steroids. J Am Chem Soc. 1952;74(1):80–8.
50. Lykidis A, Mavromatis K, Ivanova N, Anderson I, Land M, DiBartolo G, et al. Genome sequence and analysis of the soil cellulolytic actinomycete Thermobifida fusca YX. J Bacteriol. 2007;189(6):2477–86. Available from: https://journals.asm.org/doi/10.1128/JB.01899-06. [cited 2023 Feb 21].

Publisher's Note